

# Muon to positron conversion

MyeongJae Lee <sup>1,†</sup>  and Michael MacKenzie <sup>2,†</sup> 

<sup>1</sup> Sungkyunkwan University, Suwon 16419, Republic of Korea; myeongjaelee@skku.edu

<sup>2</sup> Northwestern University, Evanston, Illinois, 60208, USA; michaelmackenzie@u.northwestern.edu

\* Correspondence: michaelmackenzie@u.northwestern.edu

† These authors contributed equally to this work.

**Abstract:** Lepton flavor violation (LFV) has been discovered in the neutrino sector by neutrino oscillation experiments. The minimal extension of the Standard Model (SM) to include neutrino masses allows LFV in the charged sector (CLFV) at the loop-level, but at rates that are too small to be experimentally observed. Lepton number violation (LNV) is explicitly forbidden even in the minimally extended SM, so the observation of a LNV process would be unambiguous evidence of physics beyond the SM. The search for the LNV and CLFV process  $\mu^- + N(A, Z) \rightarrow e^+ + N'(A, Z - 2)$  (referred to as  $\mu^- \rightarrow e^+$  conversion) complements  $0\nu\beta\beta$  decay searches, and is sensitive to potential flavor effects in the neutrino mass generation mechanism. A theoretical motivation for  $\mu^- \rightarrow e^+$  conversion is presented along with a review of the status of past  $\mu^- \rightarrow e^+$  conversion experiments and future prospects. Special attention is paid to an uncertain and potentially dominant background for these searches, namely, radiative muon capture (RMC). The RMC high energy photon spectrum is theoretically understudied and existing measurements insufficiently constrain this portion of the spectrum, leading to potentially significant impacts on current and future  $\mu^- \rightarrow e^+$  searches.

**Keywords:** Muon; muon conversion; charged lepton flavor violation; CLFV; lepton number violation; LNV; radiative muon capture

## 1. Introduction

The incoherent conversion of a negative muon into a positron in a muonic atom,  $\mu^- + N(A, Z) \rightarrow e^+ + N'(A, Z - 2)$  (referred to as  $\mu^- \rightarrow e^+$  hereafter), is an exotic process that is both lepton flavor violating (LFV) and lepton number violating (LNV) with a change in lepton number by two units ( $\Delta L = 2$ ). The conservation of charged lepton number and flavor has been very well experimentally established. The symmetry corresponding to the conservation of lepton flavor is broken in the Standard Model (SM) by the introduction of neutrino masses, and the symmetry corresponding to the conservation of lepton number can additionally be broken by the introduction of new interactions and particles. In the last few decades, LFV decays of the muon have been studied experimentally through three processes, each forbidden before the introduction of neutrino masses:  $\mu^+ \rightarrow e^+\gamma$ ,  $\mu^+ \rightarrow e^+e^-e^+$ , and  $\mu^- + N \rightarrow e^- + N$  (referred to as  $\mu^- \rightarrow e^-$ ). Experiments searching for  $\mu^- \rightarrow e^-$  can also typically search for  $\mu^- \rightarrow e^+$ , and so are able to investigate both LFV and LNV in the muon sector. The most recent result on muon LFV processes comes from the MEG experiment searching for  $\mu^+ \rightarrow e^+\gamma$ , reporting  $B(\mu^+ \rightarrow e^+\gamma) < 4.2 \times 10^{-13}$  at 90% confidence level (CL) [1]. The upgrade of the MEG experiment to improve the experimental sensitivity by an order of magnitude is in progress [2]. The new Mu3e [3] at PSI will search for  $\mu^+ \rightarrow e^+e^-e^+$ , improving the sensitivity by three orders of magnitude in Phase I. New results for  $\mu^- \rightarrow e^-$  with 100 - 10,000 times better sensitivity are expected by the end of the decade from the COMET [4] and Mu2e [5] experiments.

The theoretical branching ratio expectations for muon LFV decays in the SM minimally extended to include neutrino masses are extremely small, below  $10^{-50}$  for all three searched for



**Citation:** Muon to positron conversion. *Preprints* 2021, 1, 0. <https://doi.org/>

Received:

Accepted:

Published:

**Publisher's Note:** MDPI stays neutral with regard to jurisdictional claims in published maps and institutional affiliations.

processes. The rate is suppressed by  $((\Delta m_\nu^2)/M_W^2)^2$  where  $m_\nu$  is the neutrino mass and  $M_W$  is the  $W$ -boson mass [6], and also due to the GIM (Glashow–Iliopoulos–Maiani) mechanism. Therefore, observation of any charged LFV (CLFV) process is direct evidence of physics beyond the SM.

In the LNV case, such as  $\mu^- \rightarrow e^+$ , the process is not allowed as a perturbative process. The minimal extension of the SM with a Majorana neutrino allows for the famous LNV process, neutrinoless double-beta decay ( $0\nu\beta\beta$ ), to occur. In fact, the Feynman diagrams for  $\mu^- \rightarrow e^+$  and  $0\nu\beta\beta$  mediated by a Majorana neutrino are very similar, as depicted in Figure 1, except that  $\mu^- \rightarrow e^+$  also involves a change of lepton flavor. The  $\mu^- \rightarrow e^+$  and  $0\nu\beta\beta$  processes are complimentary in the sense that  $0\nu\beta\beta$  involves same-flavor (or “flavor-diagonal”) transitions while  $\mu^- \rightarrow e^+$  involves a different flavor (of “flavor-off-diagonal”) transition. In some theories for physics beyond the SM, flavor-diagonal transitions are suppressed and observable signals of new physics are associated with different-flavor processes.

Benefiting from progress in detector technology and the feasibility of obtaining a large amount of target material, models involving LNV in general are more easily observable at  $0\nu\beta\beta$  experiments, such as KamLAND-Zen [7], than in  $\mu^- \rightarrow e^+$  searches. This is true for the case that a light Majorana neutrino mediates the LNV, where  $0\nu\beta\beta$  would be more easily measurable than  $\mu^- \rightarrow e^+$ . The effect on the  $0\nu\beta\beta$  and  $\mu^- \rightarrow e^+$  processes in a specific new physics model, for example, a heavy sterile neutrino model, is not very well studied. The “Black box theorem” [8–11] relates the Majorana neutrino mass to the amplitude of  $0\nu\beta\beta$  and any  $\Delta L = 2$  processes even in the presence of new physics, showing that the occurrence of any  $\Delta L = 2$  process, including  $\mu^- \rightarrow e^+$ , implies a nonzero Majorana neutrino mass. An enhancement or suppression of the rate of  $\mu^- \rightarrow e^+$  over  $0\nu\beta\beta$  was suggested by some new physics models [12–18]. In addition, some theories explain the LNV of  $0\nu\beta\beta$  without a Majorana neutrino exchange, but instead using a new mediator particle from a supersymmetric theory or a Majoron: see the discussion by Engel and Menéndez [19]. These models discussed by Engel and Menéndez can also be used to describe  $\mu^- \rightarrow e^+$ . Therefore, from one perspective,  $\mu^- \rightarrow e^+$  is a LNV search mediated by a Majorana neutrino similar to  $0\nu\beta\beta$  experiments, and from another perspective, it is a new physics search regarding the flavor effect on the neutrino mixing in the framework of the theory beyond the SM. While there are other LNV searches such as  $\tau^- \rightarrow e^+\pi^-\pi^-$  [20] or  $K^\pm \rightarrow \pi^\mp\mu^\pm\mu^\pm$  [21], those are not similar processes to  $0\nu\beta\beta$  or  $\mu^- \rightarrow e^+$ , so their direct comparison with  $\mu^- \rightarrow e^+$  or  $0\nu\beta\beta$  is very difficult. A few very recent studies have suggested comparing the  $0\nu\beta\beta$  results with the collider experimental results for the  $t$ -channel process of same-sign  $W$ -boson scattering [22–24].

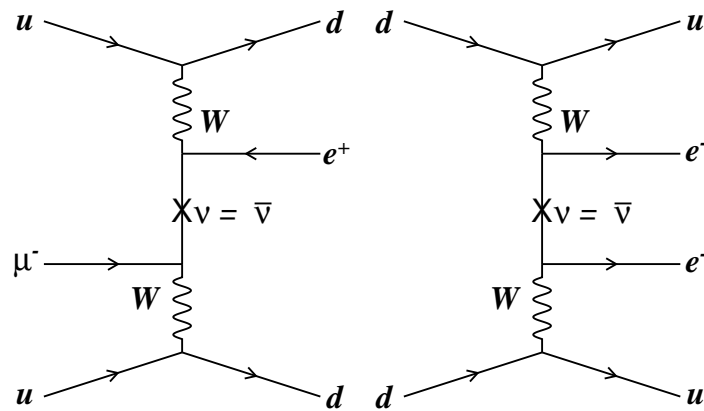


**Figure 1.** The tree level diagram of  $\mu^- \rightarrow e^+$  (left) and  $0\nu\beta\beta$  (right) in a Majorana neutrino model.

From the experimental point of view,  $\mu^- \rightarrow e^+$  is attracting more interest as the future  $\mu^- \rightarrow e^-$  experiments progress. The COMET [4] and Mu2e [5] experiments will search for  $\mu^- \rightarrow e^-$  with an experimental sensitivity down to  $10^{-17}$ . Although the experimental designs were not optimized for  $\mu^- \rightarrow e^+$ , these experiments can significantly improve the sensitivity reach of  $\mu^- \rightarrow e^+$  owing to the considerable increase in the number of muons. The current best experimental limits on  $\mu^- \rightarrow e^+$  were obtained by the SINDRUM II experiment with titanium nuclei:  $B(\mu^- + \text{Ti} \rightarrow e^+ + \text{Ca}) < 1.7 \times 10^{-12}$  at 90% CL to the ground state of calcium [25].

The purpose of this article is to emphasize the importance of the search for  $\mu^- \rightarrow e^+$  and assess its feasibility in future  $\mu^- \rightarrow e^-$  experiments. Section 2 reviews the theoretical estimation of the  $\mu^- \rightarrow e^+$  rate in connection with the  $0\nu\beta\beta$  search. It also describes the past experimental results for  $\mu^- \rightarrow e^+$ . Section 3 introduces the future  $\mu^- \rightarrow e^-$  experiments where  $\mu^- \rightarrow e^+$  can be studied. A major background component is analyzed and a mitigation strategy for suppressing the background in order to improve the signal sensitivity of  $\mu^- \rightarrow e^+$  searches is also described.

## 2. Theories and past results

### 2.1. Estimation of the $\mu^- \rightarrow e^+$ rate in the extended SM with a Majorana neutrino

A generic model of neutrino masses includes at least three light, left-handed neutrinos, with neutrino flavor oscillations described by the Pontecorvo–Maki–Nakagawa–Sakata (PMNS) matrix [26–28]. A right-handed neutrino, or any other hypothetical neutrino, may have significantly larger mass than the light neutrinos, as is expected, for example, from the Seesaw Mechanism [29–34]. In the minimal extension of the SM with a Majorana neutrino, the  $\mu^- \rightarrow e^+$  process is allowed through a light or heavy Majorana neutrino exchange, as depicted in Figure 1. But, as described before, it is also possible that other new particles beyond the SM or new interactions between quarks and leptons may mediate the interaction.

Assuming the light or heavy Majorana neutrino exchange interaction, the leading order  $\mu^- \rightarrow e^+$  matrix element when the initial and final states of nuclei are both ground states can be written as [35]:

$$\begin{aligned} \mathcal{M}_{fi} &= -i \left( \frac{G_F}{\sqrt{2}} \right)^2 \frac{1}{(2\pi)^{3/2}} \frac{1}{\sqrt{4E_{\mu^-} E_{e^+}}} \bar{v}(k_{e^+}) (1 + \gamma_5) u(k_{\mu^-}) \\ &\times \frac{m_e g_A^2}{2\pi R} \left[ \frac{\langle m_\nu \rangle_{\mu e}}{m_e} \mathcal{M}_\nu + \langle M_N^{-1} \rangle_{\mu e} m_p \mathcal{M}_N \right] \times 2\pi \delta(E_{\mu^-} + E_i - E_f - E_{e^+}) \quad (1) \\ &\propto \begin{cases} \langle m_\nu \rangle_{\mu e} \mathcal{M}_\nu & \text{(light neutrino)} \\ \langle M_N^{-1} \rangle_{\mu e} \mathcal{M}_N & \text{(heavy neutrino)} \end{cases} \end{aligned}$$

In this equation,  $G_F$  is the Fermi constant,  $m_e$  is the electron mass,  $g_A$  is the weak axial coupling constant, and  $R$  is the nuclear radius.  $E_{(\mu^-, e^+, f, i)}$  represent the energy of the muon, positron, final nuclear ground state, and initial nuclear ground state, respectively. The effective neutrino masses are defined as:

$$\langle m \rangle_{\alpha\beta} = \sum_k U_{\alpha k} U_{\beta k} m_k, \quad (2)$$

for the light neutrino, and

$$\langle M_N^{-1} \rangle_{\alpha\beta} = \sum_k \frac{U_{\alpha k} U_{\beta k}}{M_k}, \quad (3)$$

for the heavy neutrino, where  $\alpha$  and  $\beta$  are flavor indexes, and  $m_k$  and  $M_k$  represent the light neutrino mass and the heavy neutrino mass, respectively.  $U$  is the neutrino mixing matrix, or PMNS matrix for the light neutrino case. The effective neutrino mass matrix can be calculated from the current estimation of the neutrino masses and mixing angles, in the case of the light neutrino exchange model. For example, from a cosmological observation, the sum of three light neutrino masses is less than 0.42 eV, which translates to  $\langle m_\nu \rangle_{l_1 l_2} < 0.14$  eV [36].

Another important term in Equation 1 is  $\mathcal{M}_{\nu/N}$ , representing the nuclear matrix element (NME) for the light and heavy neutrino, respectively. This is a transition probability matrix of the nucleon from the initial state to the final state:

$$\mathcal{M}_i \propto \int dq \sum_n \langle f | J^\mu(x) | n \rangle \langle n | J^\nu(y) | i \rangle = \mathcal{M}_i^{(GT)} + \mathcal{M}_i^{(T)} + \mathcal{M}_i^{(F)}, \quad (4)$$

where  $n$  is an intermediate nuclear state and  $q$  and  $J$  represent the momentum transfer and hadronic current, respectively. Theoretically, the matrix element is the sum of three components: the axial vector ( $\mathcal{M}_i^{(GT)}$ , Gamow-Teller term), tensor ( $\mathcal{M}_i^{(T)}$ ), and vector ( $\mathcal{M}_i^{(F)}$ , Fermi term) terms, where the axial vector NME is the dominant one [19,37]. Because of uncertainties in the nucleus models, and difficulty of calculating many body dynamics, the NME calculation usually needs to be approximated. Approximation methods of NME calculations used for  $0\nu\beta\beta$  experiments, such as the interacting shell model (ISM), quasiparticle random-phase approximation (QRPA), interacting boson model (IBM), projected Hartree-Fock-Bogoliubov model (PHFB), and energy density functional method (EDF), are reviewed by Vergados et al. [38] and Engel and Menéndez [19]. Engel and Menéndez [19] also show the NME calculations for  $0\nu\beta\beta$  in different materials and with different approximation methods differ by up to a factor of three. This shows the importance of understanding the NME for the  $0\nu\beta\beta$  process, and therefore for the similar  $\mu^- \rightarrow e^+$  process, in the minimal extension of the SM with a Majorana neutrino.

Using this formulation, the theoretical estimation of the  $\mu^- \rightarrow e^+$  rate was obtained by Domin et al. [35]:

$$\begin{aligned} \mathcal{R}^{\mu^- e^+} &\equiv \frac{\Gamma(\mu^- + N(A, Z) \rightarrow e^+ + N'(A, Z - 2))}{\Gamma(\mu^- + N(A, Z) \rightarrow (\text{All muon captures}))} \\ &= 2.6 \times 10^{-22} \times \left\{ \begin{array}{l} |\langle m_\nu \rangle_{\mu e} / m_e|^2 |\mathcal{M}_\nu|^2 \quad (\text{light neutrino}) \\ |\langle M_N^{-1} \rangle_{\mu e m_p}|^2 |\mathcal{M}_N|^2 \quad (\text{heavy neutrino}) \end{array} \right\} \end{aligned} \quad (5)$$

Applying the effective neutrino mass obtained from the experimental data on the neutrinos masses and their mixing, and the NME for titanium from the QRPA method,  $\mathcal{R}^{\mu^- e^+}(\text{Ti})$  is:

$$\begin{aligned} &(0.008 - 1.7) \times 10^{-41} \quad \text{for a light neutrino, normal neutrino mass hierarchy,} \\ &(0.05 - 6.7) \times 10^{-40} \quad \text{for a light neutrino, inverted neutrino mass hierarchy, and} \\ &\leq 3.8 \times 10^{-24} \quad \text{for a heavy neutrino.} \end{aligned}$$

While the estimated  $\mu^- \rightarrow e^+$  rate is much higher in the heavy Majorana neutrino case than the light neutrino one, it is far smaller than the feasible experimental reach.

Any  $\Delta L = 2$  interaction other than the tree-level interaction depicted in Figure 1 may lead to  $\mu^- \rightarrow e^+$ . This was studied by Berryman et al. [12] by using an effective operator description and normalizing the estimation of the Majorana neutrino exchange case (including one- and two-loop corrections) with the above tree-level calculation. The conversion rate was estimated according to the new physics energy scale ( $\Lambda$ ), shown in Figure 2. From the expected sensitivity of Mu2e, the new physics energy scale accessible from a  $\mu^- \rightarrow e^+$  measurement

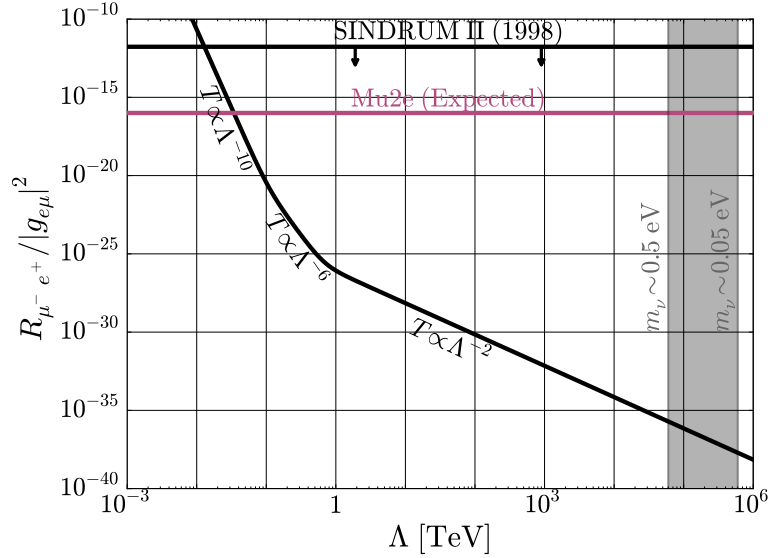


**Figure 2.** The estimation of the  $\mu^- \rightarrow e^+$  rate, as a function of the new physics scale parameter  $\Lambda$ , taken from Ref. [12].

is comparably low, around 40 GeV, compared to the new physics scale accessible from a  $\mu^- \rightarrow e^-$  measurement at Mu2e of  $\mathcal{O}(10^4)$  TeV. For all possible  $\Delta L = 2$  interactions leading to  $\mu^- \rightarrow e^+$  and  $0\nu\beta\beta$ , the new physics scale reach of  $\mu^- \rightarrow e^+$  searches is a few orders of magnitude smaller than  $0\nu\beta\beta$  experiments. According to Berryman et al. [12], the observation of  $\mu^- \rightarrow e^+$  would imply that: first, the neutrino is a Majorana fermion; second, flavor effects suppress  $0\nu\beta\beta$  while enhancing  $\mu^- \rightarrow e^+$ ; and third, a combination of complex interactions other than the tree-level interaction is responsible for the physics of nonzero neutrino mass.

## 2.2. Past $\mu^- \rightarrow e^+$ experiments

The results from past  $\mu^- \rightarrow e^+$  experiments are listed in Table 1 [39]. The experimental techniques were similar for most all of these searches: a muon beam interacted with a nuclear target, where muons quickly fell to a 1s orbit in a target atom. The outgoing positron spectrum from the nuclear target was measured in a tracking detector, searching for the  $\mu^- \rightarrow e^+$  signal. The experiment using  $^{127}\text{I}$  as the nuclear target [40] used a radiochemical method: a muon beam interacted with a NaI target, and then the target was chemically treated to extract  $^{127}\text{Sb}$  or  $^{127}\text{Te}$ , where the decay rate of  $^{127}\text{Te}$  was measured to detect an excess of  $^{127}\text{Sb}$ .

Figure 3 shows the most recent  $\mu^- \rightarrow e^+$  experimental search [25] and the comparison to the most recent  $\mu^- \rightarrow e^-$  search [41], both from SINDRUM II. For  $\mu^- \rightarrow e^+$ , the nucleus in the final state can be either in the ground state or an excited state. In the case of the transition to the ground state, the signal positron is mono-energetic with an energy ( $E_{\mu^- e^+}$ ) given by:

$$E_{\mu^- e^+} = m_\mu + M(A, Z) - M(A, Z - 2) - B_\mu - E_{\text{recoil}}, \quad (6)$$

where  $m_\mu$  is the muon mass,  $M(A, Z)$  is the mass of the nucleus  $N(A, Z)$ ,  $B_\mu$  is the binding energy of the muonic atom, and  $E_{\text{recoil}}$  is the recoil energy of the outgoing nucleus. Similarly to photo-nuclear reactions, the  $\mu^- \rightarrow e^+$  process may leave the target nuclei in an excited state, a Giant Dipole Resonance (GDR), which is a collective vibration of protons against neutrons with a dipole spatial pattern [42]. For example, a GDR with a 20 MeV width was

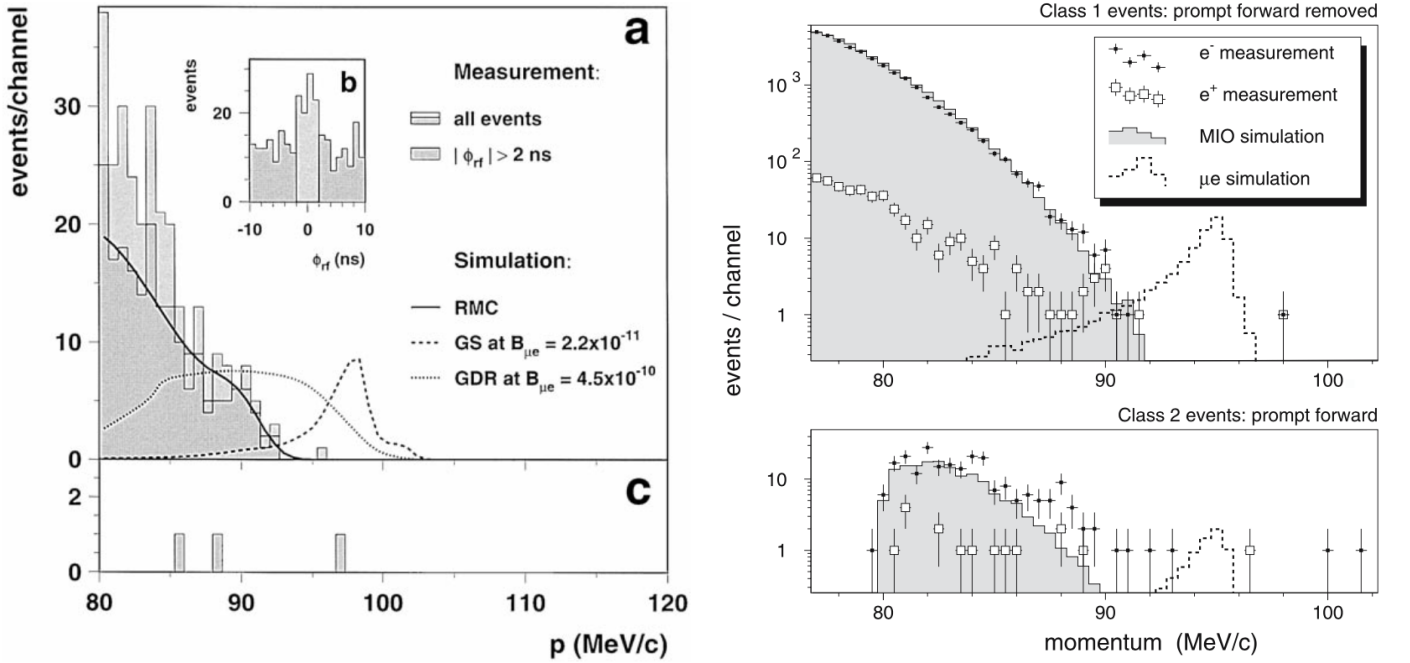


**Figure 3.** The energy spectrum of the signal estimation and backgrounds of  $\mu^- \rightarrow e^+$  (left) and  $\mu^- \rightarrow e^-$  (right) from the SINDRUM II experiment [25,41]. For  $\mu^- \rightarrow e^+$ , the and lower plots are the data when the muon beam is on and off, respectively. For  $\mu^- \rightarrow e^-$ , the and lower plots are the data with the radiative pion background candidates removed and enhanced, respectively.

**Table 1.** The past  $\mu^- \rightarrow e^+$  experimental results [39]. The limits are quoted at 90% CL, and  $N_{\text{capture}}$  is the number of muon captures in the experiments. GS and GDR represent ground state and giant dipole resonance excitation of the final nucleus status. While the natural abundance of  $^{32}\text{S}$  and  $^{127}\text{I}$  among their isotopes are almost 100%, Ti and Cu are not, which is the reason for not specifying the mass of Ti and Cu.

Nuclei	Upper limit	$N_{\text{capture}}$	Year	Experiment	Detector	GS/GDR	Reference
Ti	$3.6 \times 10^{-11}$	$2.5 \times 10^{13}$	1998	SINDRUM II	Drift chamber	GDR	[25,43]
	$1.7 \times 10^{-12}$					GS	
	$8.9 \times 10^{-11}$	$4.9 \times 10^{12}$	1993	SINDRUM II	Drift chamber	GDR	[44]
$4.3 \times 10^{-12}$	GS						
$^{32}\text{S}$	$1.7 \times 10^{-10}$	$9 \times 10^{12}$	1988	(TRIUMF)	TPC	GDR	[45]
	$9 \times 10^{-10}$	$6.7 \times 10^{11}$	1980	SIN	Streamer chamber	GDR	[46]
	$1.5 \times 10^{-9}$	$1.2 \times 10^{11}$	1978	SIN	Streamer chamber	GDR	[47,48]
Cu	$2.6 \times 10^{-8}$	$2.2 \times 10^9$	1972	(CERN)	Spark chamber	GS/GDR	[49]
	$2.2 \times 10^{-7}$		1962		Spark chamber		[50]
$^{127}\text{I}$	$3 \times 10^{-10}$	$2.1 \times 10^{12}$	1980		Radiochemical	GS	[40]

assumed in Ref. [25], resulting in a much wider energy distribution for the signal positron, as can be seen in Figure 3. The past experimental results in Table 1 are separately reported for the final ground state and GDR state of the nucleus. Table A2 lists the  $E_{\mu^-e^+}$  of the ground state transition for some selected nuclei used by or considered for  $\mu^- \rightarrow e^+$  experiments.

### 3. Future $\mu^- \rightarrow e^+$ experimental searches

#### 3.1. Upcoming experimental prospects

The COMET Phase-I [4] and Mu2e [5] experiments will have unprecedented sensitivity to  $\mu^- \rightarrow e^+$  using aluminum as their nuclear targets, with single event sensitivities (SES) on the order of  $10^{-15}$  and  $10^{-17}$  respectively in the  $\mu^- \rightarrow e^-$  conversion search. These experiments are expected to have similar sensitivities in the  $\mu^- \rightarrow e^+$  channel. After COMET Phase-I, the detector will be upgraded for COMET Phase-II which will have an SES on the order of  $10^{-17}$  [4]. COMET Phase-II will not be able to search for positron and electron signals simultaneously, so a  $\mu^- \rightarrow e^+$  search would be a special run of the  $\mu^- \rightarrow e^-$  experiment and not necessarily reach the same muon statistics as estimated for the electron channel. There has also been an expression of interest in upgrading the Mu2e detector, called Mu2e-II, with an SES on the order of  $10^{-18}$  [51].

Both COMET Phase-I and Mu2e use similar principles to search for the  $\mu^- \rightarrow e^-$  and  $\mu^- \rightarrow e^+$  processes: (1) a pulsed proton beam is used to produce pions and muons in a production target within a superconducting solenoid; (2) the low momentum pions and muons are guided by the superconducting production solenoid field to a curved transport superconducting solenoid, which has an acceptance designed to eliminate high momentum particles; (3) an off-axis collimator selects the desired charge of the beam, utilizing the sign-dependent drift of the beam along the curved beamline; (4) the muons from production and pion decays along the beamline are stopped in a nuclear target within a superconducting solenoid containing the cylindrical detector elements; (5) non-stopped beam particles continue through the solenoid, passing through a central axis hole in the detector elements; (6) after a time sufficient for nearly all pions to either decay or be captured on the nuclear target, signal candidates are reconstructed in the detectors (where the central holes blind them to the high intensity, low momentum muon decay backgrounds). COMET Phase-II is similar to Phase-I, except after the stopping target there is a second curved transport solenoid followed by the detectors, where the second transport solenoid provides the momentum filtering, eliminating the need for a central hole in the detectors. This second transport solenoid is also what prevents the simultaneous search for  $\mu^- \rightarrow e^-$  and  $\mu^- \rightarrow e^+$ . The pulsed proton beam significantly reduces beam related backgrounds during the signal measurement period by delaying the signal measurement period until after the beam products arrive. This time delay method requires that the lifetime of the muon in the nuclear target (see Table A2) is large enough that there are a sufficient number of muon captures/decays in the target during the signal search period. Due to this restriction, nuclear target materials with  $Z \gtrsim 40$  cannot be easily studied at experiments like COMET and Mu2e.

#### 3.2. Background consideration

A potentially dominant physics background to  $\mu^- \rightarrow e^+$  comes from radiative muon capture (RMC),

$$\mu^- + N(A, Z) \rightarrow \nu_\mu + N(A, Z - 1) + \gamma,$$

followed by photon pair production,  $\gamma \rightarrow e^+e^-$ , where the  $e^+$  in the pair is misidentified as a signal. The photon energy spectrum of RMC, in particular in the endpoint energy region, is poorly known experimentally [52]. However, the maximum allowed endpoint energy ( $E_{\text{RMC}}^{\text{end}}$ ) can be kinematically determined:

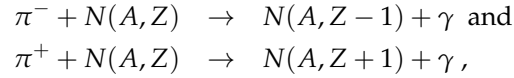
$$E_{\text{RMC}}^{\text{end}} = m_\mu + M(A, Z) - M(A, Z - 1) - B_\mu - E_{\text{recoil}}. \quad (7)$$

The endpoint energies of some relevant nuclei are shown in Table A2. The nucleus in the final state may not be  $N(A, Z - 1)$  once nucleon emission occurs. In this case, the RMC

endpoint energy is smaller than that of Equation 7. It is also possible that the RMC endpoint energy could be much smaller depending on the spin state of the  $N(A, Z)$  and  $N(A, Z - 1)$  nuclei. In order to account for the RMC background, it is necessary to measure the RMC photon spectrum, either at the  $\mu^- \rightarrow e^-$  experiment or in a dedicated experiment, such as the AlCap experiment [53]. In addition, the kinematic separation of the RMC background and the  $\mu^- \rightarrow e^+$  positron can be improved in future experiments such as COMET Phase-II or Mu2e-II by choosing a target material where the endpoint energy of RMC is smaller than the  $\mu^- \rightarrow e^+$  positron energy,  $E_{\text{RMC}}^{\text{end}} < E_{\mu^- e^+}$  [54], therefore:

$$M(A, Z - 2) < M(A, Z - 1). \quad (8)$$

Radiative pion capture (RPC),



followed by  $\gamma \rightarrow e^+e^-$  is another background source, when the converted positron is misidentified as a signal. The RPC background can be controlled in  $\mu^- \rightarrow e^+$  and  $\mu^- \rightarrow e^-$  experiments by suppressing the pion contamination in the muon beam. The pion contamination can be suppressed by using a beamline sufficiently long where the pions decay to muons before reaching the nuclear target. This was true for the previous  $\mu^- \rightarrow e^-$  measurements, where the  $\pi/\mu$  ratio was about  $10^{-7}$  for the SINDRUM II experiment for example, allowing the use of a continuous muon beam with continuous data acquisition [25]. The COMET and Mu2e  $\mu^- \rightarrow e^-$  experiments are targeting a factor of 100 to 10,000 improvement on the upper limits for the  $\mu^- \rightarrow e^-$  process in the absence of a signal. To suppress the effects of pions and other non-muon beam particles contaminating the beam, they are adopting a pulsed proton beam with a high inter-beam pulse primary particle suppression and a delayed data acquisition timing window technique [4,5].

Antiprotons contaminating the muon beam can annihilate in the muon stopping target and create high energy background  $e^\pm$  tracks, as well as introduce delayed pion background due to interactions along the muon beamline. Along with the pulsed beam technique, antiproton absorbers can be placed in the muon beamline to suppress the antiproton background.

Another large background arises from cosmic-ray induced events. In general, the cosmic-ray induced background is similar for the  $\mu^- \rightarrow e^-$  and  $\mu^- \rightarrow e^+$  searches. Therefore, the consideration of the detector design to suppress the cosmic-ray background for the  $\mu^- \rightarrow e^-$  search is also applicable for the  $\mu^- \rightarrow e^+$  search. The COMET and Mu2e experiments are developing cosmic-ray veto detector systems to detect charged cosmic-ray particles entering the detectors and veto signal candidates coincident with these detected cosmic-rays. Cosmic-rays can be reconstructed in the trackers at COMET Phase-I and Mu2e to constrain the cosmic-ray veto detector systems' efficiencies, and in the case of COMET Phase-I where the tracking detector covers the muon stopping target, cosmic-rays that interact with the stopping target and produce background tracks can be fully reconstructed [55].

Muon decay-in-orbit (DIO), which is one of the major background sources for  $\mu^- \rightarrow e^-$ , is also a background source in the  $\mu^- \rightarrow e^+$  search due to photons generated in DIO electron interactions pair-creating a positron in the detector material. It is not an important background at the SES of the planned COMET and Mu2e experiments as long as the charge identification is sufficient to suppress DIO electrons being reconstructed as positron events. However, it should be noted that the charge identification will never be perfect, especially in the case that an electron or positron is generated downstream of the detector system and propagates back to the muon stopping target, where only the tracker hit timing and, for Mu2e and COMET Phase-II, the calorimeter information can distinguish the particle trajectory.



### 3.3. RMC status

Both COMET and Mu2e will have far greater sensitivity to the high momentum positron spectrum from RMC than previous muon conversion and RMC measurement experiments. The background to the  $\mu^- \rightarrow e^+$  search arises from highly asymmetric RMC photon conversions, either from on-shell photons converting in the detector material or off-shell photons internally converting, and the background strongly depends on the nuclear target. The internal conversion spectrum for RMC has never been measured, though the internal conversion spectrum approximation from Kroll and Wada [56] (with corrections published by Joseph [57]) for general nuclear captures with RPC in mind should similarly apply for RMC, as shown by Plestid and Hill [58]. This approximation makes simplifying assumptions about the  $e^+e^-$  matrix element by using the energy spectrum of the on-shell photon and assumes that the virtuality of the  $e^+e^-$  pair is small. Following this, the internal conversion spectrum can be estimated directly from the on-shell photon spectrum, requiring only an on-shell photon spectrum to predict the total on- and off-shell photon induced background. Plestid and Hill show that this approximation is most reliable in the high energy region of the positron spectrum, with the next order uncertainty decreasing as the positron energy approaches the endpoint [58].

The on-shell RMC photon spectrum was measured by the TRIUMF RMC Spectrometer group on several nuclear targets, including aluminum [52,59–61]. The experiment was interested in studying the pseudoscalar coupling constant in weak interactions,  $g_p$ , through the ratio  $g_p/g_a$ , where  $g_a$  is the axial coupling constant. As such, the focus of the measurements was on the total rate of RMC, not on a precise model of the high energy tail.

The closure approximation is typically used to describe the RMC photon energy spectrum, where one assumes the sum of the nuclear final states can be approximated with a single nuclear transition using the mean excitation energy. This nuclear excitation energy manifests as the closure approximation endpoint, and is typically considered a free parameter that is fit to data. The closure approximation photon energy spectrum is shown in Equation 9, where  $x = E_\gamma/k_{\max}$  and  $k_{\max}$  is the spectrum endpoint [62]:

$$\frac{dn}{dx} = \frac{e^2 k_{\max}^2}{\pi m_\mu^2} \left(1 - \frac{N-Z}{A}\right) (1 - 2x + 2x^2)x(1-x)^2. \quad (9)$$

The TRIUMF RMC Spectrometer group measured a closure approximation endpoint of  $90.1 \pm 1.8$  MeV and a branching fraction of  $(1.40 \pm 0.11) \times 10^{-5}$  above 57 MeV with respect to ordinary muon capture (OMC) using aluminum as their nuclear target [52]. This endpoint is significantly lower than the kinematic endpoint on aluminum,  $\sim 101.9$  MeV, as shown in Appendix A. This was the case for all of the nuclear targets – the fit closure approximation endpoint was  $\sim 10$  MeV below the target’s kinematic endpoint. As nothing forbids photon energies up to the kinematic endpoint, there is no reason to expect the spectrum to be 0 between the measured endpoint and the kinematic endpoint, though it may be suppressed. Predictions using a Fermi gas model by Fearing et al. [63,64] show the photon energy spectrum falling up to the kinematic endpoint, with no tuned endpoint as found in the closure approximation. A few example spectra from these calculations are shown in Figure 4.

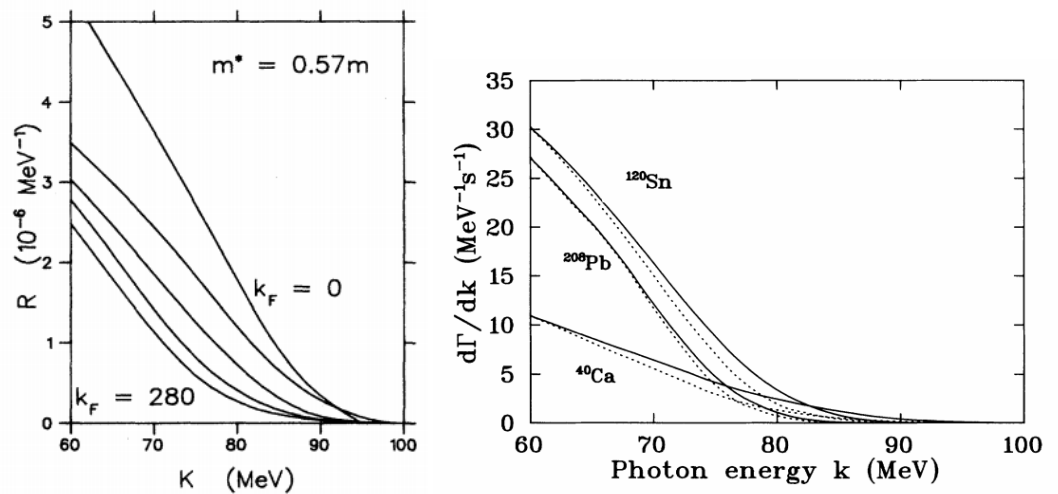


**Figure 4.** RMC spectra vs  $k_{\text{Fermi}}$  [63] (left) and example RMC spectra [64] (right) as calculated using a Fermi gas model.

On aluminum, the nuclear target for the currently planned COMET Phase-I and Mu2e searches, the ground state transition energy for the positron signal is 92.3 MeV, far below the RMC kinematic endpoint of  $\sim 101.9$  MeV. Unlike the  $\mu^- \rightarrow e^-$  searches, DIO backgrounds are not a significant background in the positron channel at the sensitivity level of the current and future experiments, so the dominant backgrounds are RMC, RPC, antiprotons, and cosmic-ray events. The non-RMC backgrounds are expected to contribute similarly in the positron and electron channel, where the expectation is less than 1 event per experiment for both searches [4,5]. Assuming the closure approximation with the measured endpoint, the true positron spectrum would end at  $89.6 \pm 1.8$  MeV/c with a rapidly falling spectrum, so only resolution and energy loss effects would lead to overlaps with the signals. As the resolution is approximately 200 keV/c for both experiments [4,5] and the two processes are separated by nearly 3 MeV/c, both experiments would be able to maintain a background expectation of below 1 event per experiment for the measured endpoint.

The dataset on aluminum for the 1999 RMC measurement from TRIUMF only had 3,051 photons above 57 MeV, so this measurement was not sensitive to photon rates above 90 MeV that are about 3,000 times smaller than the total rate above 57 MeV ( $R(E_\gamma > 57 \text{ MeV}) = \frac{\Gamma_{\text{RMC}}(E_\gamma > 57 \text{ MeV})}{\Gamma_{\text{OMC}}}$ ). COMET Phase-I and Mu2e will see about  $10^{16}$  and  $10^{18}$  muon captures respectively [4,5], and so will have  $\sim 10^{11}$  and  $10^{13}$  RMC photons above 57 MeV. To test their sensitivity to RMC beyond the fit endpoint on aluminum, we assume a flat photon energy spectrum tail above 90 MeV up to the kinematic endpoint with a rate around the sensitivity limit of the 1999 measurement, shown in Equation 10:

$$R(E_\gamma > 90 \text{ MeV}) = \frac{1}{3,000} \times R(E_\gamma > 57 \text{ MeV}) = 4.7 \times 10^{-9} . \quad (10)$$

We also make the following simplifying assumptions: all  $e^\pm$  energies from a photon conversion are equally likely, such that the energy sharing distribution between the  $e^+e^-$  pair is flat, there is a 0.1% chance of a photon conversion in the nuclear target, and the tracking efficiency for  $\sim 90$  MeV/c positrons is 10%. This leads to a positron background rate of  $\mathcal{O}(500)$  and  $\mathcal{O}(50,000)$  events per MeV/c at 90 MeV/c for COMET Phase-I and Mu2e respectively, before considering internal photon conversions, as shown in Figure 5. In this simple model, which is consistent with the existing data on aluminum, the RMC background estimate would change

from below 1 background event to tens of thousands of background events near the signal for  $10^{18}$  muon captures, significantly lessening the discovery potential of  $\mu^- \rightarrow e^+$  signal searches.

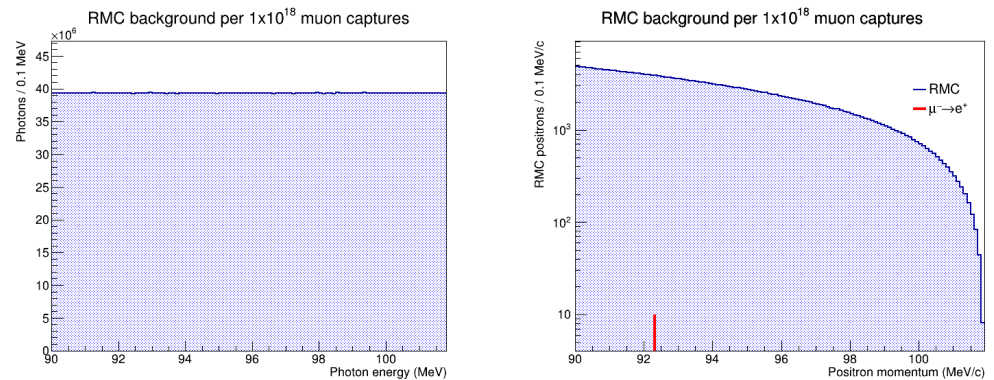


**Figure 5.** Assumed on-shell RMC photon spectrum high energy tail on aluminum for  $10^{18}$  muon captures (left) and the corresponding positron spectrum using the simplifying assumptions about the conversion spectrum and track reconstruction (right). The signal process is also shown using the same tracking efficiency for a sample  $\mathcal{R}^{\mu^- e^+}$  value of  $10^{-16}$ , which would likely be discoverable in the absence of an RMC background.

#### 3.4. RMC considerations at future $\mu^- \rightarrow e^+$ experiments

The discovery potential of future experiments searching for  $\mu^- \rightarrow e^+$  is entwined with their understanding of the RMC background, where any claim of new physics must also be able to accurately subtract the SM background. As the RMC spectrum is not well constrained by existing measurements, muon conversion experiments should plan to perform RMC measurements on the relevant nuclear targets. COMET and Mu2e should investigate how to measure the RMC spectrum using the electron and positron spectra, paying special attention to how to avoid unblinding the  $\mu^- \rightarrow e^+$  signal region of the positron spectrum. If both the electron and positron track can be reconstructed for an RMC photon conversion, this will allow one to measure the photon energy while also likely avoiding the  $\mu^- \rightarrow e^+$  signal unblinding. A calorimeter measurement, using reconstructed photon clusters, would allow a direct measurement of the photon energy spectrum, where the positron spectrum due to off-shell conversions can be described using the results from Plestid and Hill given a measurement of the on-shell photon spectrum [58]. A dedicated experiment to measure the RMC spectrum on the intended nuclear target should also be investigated.

Future muon conversion experiments can also consider choosing a nuclear target whose  $\mu^- \rightarrow e^+$  ground state transition energy is above the kinematic endpoint of the RMC spectrum, kinematically suppressing this background. This translates into a requirement that the nuclear mass of  $N(A, Z-2)$  is smaller than the nuclear mass of  $N(A, Z-1)$ . Several potential target choices were identified by Yeo et al. [54], where all of the nuclear targets considered had  $\mu^- \rightarrow e^+$  ground state transition energies greater than the RMC positron kinematic endpoints. Example targets well suited for  $\mu^- \rightarrow e^+$  measurements are titanium (a common candidate for  $\mu^- \rightarrow e^-$  experiments), sulfur, and calcium, which satisfy this mass difference requirement while they also have long enough muon lifetimes to be useful at experiments with delayed data acquisition to suppress pion backgrounds. For each nuclear target considered, the authors assumed a closure approximation with the endpoint set to be the kinematic endpoint and the branching fraction above 57 MeV to be the measured value by the TRIUMF RMC Spectrometer group. For an example  $10^{18}$  muon stops, they found COMET Phase-II would be able to achieve limits at 90% CL of  $\mathcal{O}(10^{-15})$  for the ground state transition, a three order of magnitude improvement upon the current limit from Ref. [25]. This is compared to the

potential one order of magnitude gain by using aluminum as the nuclear target [54], showing how critical the nuclear target choice can be for the  $\mu^- \rightarrow e^+$  search.

These potential upper limits do not include an assessment of the impact on the limit due to the systematic uncertainty on the RMC background modeling. The closure approximation does not take into account exclusive transitions to low lying states, which could lead to a more complicated background spectrum with kinks or knees in the photon energy spectrum. These are likely to be smoothed by the (internal) pair conversion spectrum, but without understanding the RMC spectrum it will be difficult to have confidence that an observation of 5-10 events is definitive evidence of  $\mu^- \rightarrow e^+$  conversion, and not instead due to an RMC transition. An observation of this size is sufficient to claim a discovery at the upcoming  $\mu^- \rightarrow e^-$  searches. As the goal of these searches is to discover new physics, the experiments must be prepared for the potential discovery of the LFV and LNV process,  $\mu^- \rightarrow e^+$ , which requires the confident rejection of RMC as an alternate hypothesis.

#### 4. Concluding remarks: Towards future $\mu^- \rightarrow e^+$ measurements

CLFV is a long sought-after signal of physics beyond the SM. Many experiments have searched for  $\mu^- \rightarrow e^-$  and  $\mu^- \rightarrow e^+$  processes, where the results are complementary to the best-measured CLFV channel,  $\mu \rightarrow e\gamma$ . The  $\mu^- \rightarrow e^+$  process is also an LNV channel, which may give insight into the Majorana property of the neutrino. Although it is not as strong a channel as  $0\nu\beta\beta$  is in general, its discovery would provide insight on potential flavor effects in the neutrino mass generation. Current and future experiments will have unprecedented sensitivity to both  $\mu^- \rightarrow e^-$  and  $\mu^- \rightarrow e^+$  processes. However, the search for  $\mu^- \rightarrow e^+$  requires more careful considerations in terms of the nuclear target selection in order to reach the full discovery potential of these experiments.

RMC is one of the least understood backgrounds at  $\mu^- \rightarrow e^-$  experiments, with the potential to be the largest background in the  $\mu^- \rightarrow e^+$  search. RMC is theoretically understudied, and previous RMC measurements do not have the necessary sensitivity in the high energy photon region to sufficiently constrain this background at the currently planned COMET Phase-I and Mu2e experiments. These experiments will need to measure the RMC photon energy spectrum in order to confidently reject the SM background in the case of a  $\mu^- \rightarrow e^+$  signal.

An important consideration for the currently planned COMET and Mu2e experiments using aluminum as their nuclear target is what the next steps will be if they discover the process of  $\mu^- \rightarrow e^+$ . A common idea is to attempt to determine the nature of the new physics by testing the nuclear target dependence of the conversion rate [51]. For  $\mu^- \rightarrow e^-$ , Ref. [65] and [66] show for example models this rate may only vary by  $\sim 10\text{-}30\%$  between the models for nuclear targets feasible for COMET Phase-II and Mu2e-II. The total number of muon captures will likely only be known to  $\sim 10\%$  [5], uncorrelated between the targets, making a comparison with less than 15% uncertainty in the difference between the rates difficult. It would also require a high statistics discovery to have a precise measurement of the branching fraction, far beyond the threshold of  $\sim 5\text{-}10$  events needed to claim a discovery for the  $\mu^- \rightarrow e^-$  (and potentially  $\mu^- \rightarrow e^+$ ) searches.

In the  $\mu^- \rightarrow e^+$  case, there is more than the ground state transition to consider. Experiments can search for the GDR transition in addition to the ground-state transition, and measure the relative rate between the ground state and the GDR transition. As this is a ratio, independent of the number of muon captures, it is possible this can be better used to test the rate dependence on the nuclear target, helping to understand the underlying mechanism for the LNV process. The nuclear dependence of the  $\mu^- \rightarrow e^+$  process needs to be further studied to determine the potential next steps experiments should take in the case of a  $\mu^- \rightarrow e^+$  discovery.

## Appendix A RMC endpoint calculation on aluminum

The RMC kinematic endpoint on aluminum can be calculated by considering the “decay” of the  $\mu^- N(A, Z)$  system to  $\gamma N(A, Z - 1)\nu_\mu$  with  $p(\nu_\mu) = 0$ , which is then a two body decay with a photon energy given by Equation 7. Since the muon is  $\sim 200$  times heavier than the electron, and therefore has a much closer orbit in the atom, the electrons do not participate in the process. The relevant masses are then the muon mass and the incoming and outgoing nuclei masses, not the atomic masses, where the nuclear mass is given by  $M(A, Z) = M_A - Z \cdot m_e$ , where  $M_A = A_r \cdot u$ ,  $A_r$  is the relative mass,  $u$  is the atomic mass unit, and  $m_e$  is the electron mass. The final state particles then satisfy  $p_\gamma = -p_{27Al}$  and the energy of the recoiling magnesium nucleus is given by:

$$E_{27Mg} = \frac{M^2 + M_N(27Mg)^2}{2M} = E_{\text{recoil}} + M_N(27Mg), \quad (\text{A1})$$

where  $M$  is the mass of the muonic aluminum system,  $M = M(27Al) + m_\mu - B_\mu$ . Table A1 shows the input parameters for Equations A1 and 7. The resulting kinematic RMC endpoint on aluminum is 101.867 MeV. The corresponding positron energy endpoint that is relevant for  $\mu^- \rightarrow e^+$  experiments is one electron mass below this, which is listed in Table A2 for some example nuclei.

**Table A1.** Parameters used in the RMC endpoint energy calculation on aluminum.

Parameter	Value	Reference
$m_\mu$	105.6583745	MeV/c <sup>2</sup> [67]
$m_e$	0.5109989461	MeV/c <sup>2</sup> [67]
$1u$	931.49410242	MeV/c <sup>2</sup> [67]
$B_\mu$	0.464	MeV [68]
$A_r(27Al)$	26.98153841	u [69]
$M_N(27Al)$	25126.501	MeV/c <sup>2</sup>
$A_r(27Mg)$	26.98434063	u [69]
$M_N(27Mg)$	25129.622	MeV/c <sup>2</sup>
$E_{\text{recoil}}$	0.206	MeV/c <sup>2</sup>

**Table A2.** The energy of the signal positron ( $E_{\mu^-e^+}$ ) obtained from Equation 6, the RMC positron endpoint energy ( $E_{\text{RMC}}^{\text{end}}$ ) of the ground state transition obtained from Equation 7, and the lifetime of the muonic atom ( $\tau_{\mu^-}$ ) of some nuclei considered for  $\mu^- \rightarrow e^+$  experiments. The energy of the signal electron ( $E_{\mu^-e^-}$ ) for  $\mu^- \rightarrow e^-$  are also shown for comparison. Nuclear masses required for these calculations are taken from AME2016 data [69]. The lifetime data is from Ref. [70].

Nuclide	$E_{\mu^-e^+}$ [MeV]	$E_{\text{RMC}}^{\text{end}}$ [MeV]	$\tau_{\mu^-}$ [ns]	$E_{\mu^-e^-}$ [MeV]
<sup>27</sup> Al	92.30	101.36	864	104.97
<sup>32</sup> S	101.80	102.03	555	104.76
<sup>40</sup> Ca	103.55	102.06	333	104.39
<sup>48</sup> Ti	98.89	99.17	329	104.18

**Author Contributions:** Writing—original draft preparation, M. L. and M. M.; writing—review and editing, M.L. and M. M. All authors have read and agreed to the published version of the manuscript.

**Funding:** This research of M.L. was supported by Institute for Basic Science (IBS-R017-D1-2021-a00) of Korea. This research of M.M. was in part funded by the “Research in the Energy, Cosmic and Intensity Frontiers at Northwestern University” award, DE-SC0015910.

**Institutional Review Board Statement:** Not applicable.

**Informed Consent Statement:** Not applicable.

**Data Availability Statement:** The data used in this study can be provided by the authors upon request.

**Acknowledgments:** The authors M.L. and M.M. are collaborators of the COMET and Mu2e collaborations, respectively. The author M.L. thanks KEK and J-PARC, Japan for their support of infrastructure and the operation of COMET. This work of M.L. is supported in part by: Japan Society for the Promotion of Science (JSPS) KAKENHI Grant Nos. 25000004 and 18H05231; JSPS KAKENHI Grant No. JP17H06135; Belarusian Republican Foundation for Fundamental Research Grant F18R-006; National Natural Science Foundation of China (NSFC) under Contracts No. 11335009 and 11475208; Research program of the Institute of High Energy Physics (IHEP) under Contract No. Y3545111U2; the State Key Laboratory of Particle Detection and Electronics of IHEP, China, under Contract No. H929420BTD; Supercomputer funding in Sun Yat-Sen University, China; National Institute of Nuclear Physics and Particle Physics (IN2P3), France; Shota Rustaveli National Science Foundation of Georgia (SRNSFG), grant No. DI-18-293; Deutsche Forschungsgemeinschaft grant STO 876/7-1 of Germany; Joint Institute for Nuclear Research (JINR), project COMET #1134; Institute for Basic Science (IBS) of Republic of Korea under Project No. IBS-R017-D1-2021-a00; Ministry of Education and Science of the Russian Federation and by the Russian Fund for Basic Research grants: 17-02-01073, 18-52-00004; Science and Technology Facilities Council, United Kingdom; JSPS London Short Term Predoctoral Fellowship program, Daiwa Anglo-Japanese Foundation Small Grant; and Royal Society International Joint Projects Grant. The author M.M. is grateful for the vital contributions of the Fermilab staff and the technical staff of the participating institutions to Mu2e. This work was supported by the US Department of Energy; the Istituto Nazionale di Fisica Nucleare, Italy; the Science and Technology Facilities Council, UK; the Ministry of Education and Science, Russian Federation; the National Science Foundation, USA; the Thousand Talents Plan, China; the Helmholtz Association, Germany; and the EU Horizon 2020 Research and Innovation Program under the Marie Skłodowska-Curie Grant Agreement No. 690835, 734303, 822185, 858199. This document was prepared in part by members of the Mu2e Collaboration using the resources of the Fermi National Accelerator Laboratory (Fermilab), a U.S. Department of Energy, Office of Science, HEP User Facility. Fermilab is managed by Fermi Research Alliance, LLC (FRA), acting under Contract No. DE-AC02-07CH11359.

**Conflicts of Interest:** The authors declare no conflict of interest.

## References

- Baldini, A. M.; et al. (MEG collaboration). Search for the lepton flavour violating decay  $\mu^+ \rightarrow e^+ \gamma$  with the full dataset of the MEG experiment. *The European Physical Journal C* **2016**, *76*, 434. doi:10.1140/epjc/s10052-016-4271-x.
- Baldini, A. M.; et al. (MEG collaboration). The Search for  $\mu^+ \rightarrow e^+ \gamma$  with  $10^{-14}$  Sensitivity: The Upgrade of the MEG Experiment. *Symmetry* **2021**, *13*. doi:10.3390/sym13091591.
- Arndt K.; et al. (Mu3e collaboration). Technical design of the phase I Mu3e experiment. *Nuclear Instruments and Methods in Physics Research Section A: Accelerators, Spectrometers, Detectors and Associated Equipment* **2021**, *1014*, 165679. doi:https://doi.org/10.1016/j.nima.2021.165679.
- Abramishvili, R.; et al. (COMET collaboration). COMET Phase-I technical design report. *Progress of Theoretical and Experimental Physics* **2020**, *2020*, [https://academic.oup.com/ptep/article-pdf/2020/3/033C01/32903980/ptz125.pdf]. 033C01, doi:10.1093/ptep/ptz125.
- Bartoszek, L.; et al. (Mu2e collaboration). Mu2e Technical Design Report, 2015, [arXiv:physics.ins-det/1501.05241].
- Marciano, W.J.; Mori, T.; Roney, J.M. Charged Lepton Flavor Violation Experiments. *Annual review of nuclear and particle science* **2008**, *58*, 315–341.
- Gando, Y. First results of KamLAND-Zen 800. *Journal of Physics: Conference Series* **2020**, *1468*, 012142. doi:10.1088/1742-6596/1468/1/012142.
- Schechter, J.; Valle, J.W.F. Neutrinoless double- $\beta$  decay in  $SU(2) \times U(1)$  theories. *Phys. Rev. D* **1982**, *25*, 2951–2954. doi:10.1103/PhysRevD.25.2951.
- Nieves, J. Dirac and pseudo-Dirac neutrinos and neutrinoless double beta decay. *Physics Letters B* **1984**, *147*, 375–379. doi:https://doi.org/10.1016/0370-2693(84)90136-9.

10. Takasugi, E. Can the neutrinoless double beta decay take place in the case of Dirac neutrinos? *Physics Letters B* **1984**, *149*, 372–376. doi:[https://doi.org/10.1016/0370-2693\(84\)90426-X](https://doi.org/10.1016/0370-2693(84)90426-X).
11. Hirsch, M.; Kovalenko, S.; Schmidt, I. Extended Black box theorem for lepton number and flavor violating processes. *Physics Letters B* **2006**, *642*, 106–110. doi:<https://doi.org/10.1016/j.physletb.2006.09.012>.
12. Berryman, J.M.; de Gouvêa, A.; Kelly, K.J.; Kobach, A. Lepton-number-violating searches for muon to positron conversion. *Phys. Rev. D* **2017**, *95*, 115010. doi:10.1103/PhysRevD.95.115010.
13. Geib, T.; Merle, A.; Zuber, K.  $\mu^- - e^+$  conversion in upcoming LFV experiments. *Physics Letters B* **2017**, *764*, 157 – 162. doi:<https://doi.org/10.1016/j.physletb.2016.11.029>.
14. Geib, T.; Merle, A.  $\mu^- - e^+$  conversion from short-range operators. *Phys. Rev. D* **2017**, *95*, 055009. doi:10.1103/PhysRevD.95.055009.
15. Chen, C.S.; Geng, C.Q.; Ng, J.N. Unconventional neutrino mass generation, neutrinoless double beta decays, and collider phenomenology. *Phys. Rev. D* **2007**, *75*, 053004. doi:10.1103/PhysRevD.75.053004.
16. King, S.F.; Merle, A.; Panizzi, L. Effective theory of a doubly charged singlet scalar: complementarity of neutrino physics and the LHC. *JHEP* **2014**, *2014*, 124. doi:10.1007/JHEP11(2014)124.
17. Pritimita, P.; Dash, N.; Patra, S. Neutrinoless Double Beta Decay in LRSM with Natural Type-II seesaw Dominance. *JHEP* **2016**, *2016*, 147, [[arXiv:hep-ph/1607.07655](https://arxiv.org/abs/hep-ph/1607.07655)]. doi:10.1007/JHEP10(2016)147.
18. Cirigliano, V.; Kurylov, A.; Ramsey-Musolf, M.J.; Vogel, P. Neutrinoless Double Beta Decay and Lepton Flavor Violation. *Phys. Rev. Lett.* **2004**, *93*, 231802. doi:10.1103/PhysRevLett.93.231802.
19. Engel, J.; Menéndez, J. Status and future of nuclear matrix elements for neutrinoless double-beta decay: a review. *Reports on Progress in Physics* **2017**, *80*, 046301. doi:10.1088/1361-6633/aa5bc5.
20. Miyazaki, Y.; et al. (Belle collaboration). Search for lepton-flavor and lepton-number-violating  $\tau \rightarrow \ell h h'$  decay modes. *Physics Letters B* **2013**, *719*, 346–353. doi:<https://doi.org/10.1016/j.physletb.2013.01.032>.
21. Cortina Gil, E.; et al. (NA62 collaboration). Searches for lepton number violating  $K^+$  decays. *Physics Letters B* **2019**, *797*, 134794. doi:<https://doi.org/10.1016/j.physletb.2019.07.041>.
22. Fuks, B.; Neundorff, J.; Peters, K.; Ruiz, R.; Saimpert, M. Probing the Weinberg operator at colliders. *Phys. Rev. D* **2021**, *103*, 115014. doi:10.1103/PhysRevD.103.115014.
23. Fuks, B.; Neundorff, J.; Peters, K.; Ruiz, R.; Saimpert, M. Majorana neutrinos in same-sign  $W^\pm W^\pm$  scattering at the LHC: Breaking the TeV barrier. *Phys. Rev. D* **2021**, *103*, 055005. doi:10.1103/PhysRevD.103.055005.
24. Cirigliano, V.; Dekens, W.; de Vries, J.; Fuyuto, K.; Mereghetti, E.; Ruiz, R. Leptonic anomalous magnetic moments in  $\nu$ SMEFT. *Journal of High Energy Physics* **2021**, *2021*, 103. doi:10.1007/JHEP08(2021)103.
25. Kaulard, J.; Dohmen, C.; Haan, H.; Honecker, W.; Junker, D.; Otter, G.; Starlinger, M.; Wintz, P.; Hofmann, J.; Bertl, W.; Egger, J.; Krause, B.; Egli, S.; Engfer, R.; Findeisen, C.; Hermes, E.; Kozłowski, T.; Niebuhr, C.; Rutsche, M.; Pruijs, H.; van der Schaaf, A. Improved limit on the branching ratio of  $\mu^- \rightarrow e^+$  conversion on titanium. *Physics Letters B* **1998**, *422*, 334–338. doi:[https://doi.org/10.1016/S0370-2693\(97\)01423-8](https://doi.org/10.1016/S0370-2693(97)01423-8).
26. Pontecorvo, B. Inverse beta processes and nonconservation of lepton charge. *Zh. Eksp. Teor. Fiz.* **1957**, *34*, 247.
27. Pontecorvo, B. Mesonium and anti-mesonium. *Sov. Phys. JETP* **1957**, *6*, 429.
28. Maki, Z.; Nakagawa, M.; Sakata, S. Remarks on the Unified Model of Elementary Particles. *Progress of Theoretical Physics* **1962**, *28*, 870–880, [<https://academic.oup.com/ptp/article-pdf/28/5/870/5258750/28-5-870.pdf>]. doi:10.1143/PTP.28.870.
29. Minkowski, P.  $\mu \rightarrow e \gamma$  at a rate of one out of  $10^9$  muon decays? *Physics Letters B* **1977**, *67*, 421–428. doi:[https://doi.org/10.1016/0370-2693\(77\)90435-X](https://doi.org/10.1016/0370-2693(77)90435-X).
30. Gell-Mann, M.; Ramond, P.; Slansky, R. Complex Spinors and Unified Theories. *Conf. Proc. C* **1979**, *790927*, 315–321, [[arXiv:hep-th/1306.4669](https://arxiv.org/abs/hep-th/1306.4669)].
31. Yanagida, T. Horizontal Symmetry and Masses of Neutrinos. *Progress of Theoretical Physics* **1980**, *64*, 1103–1105, [<https://academic.oup.com/ptp/article-pdf/64/3/1103/5394376/64-3-1103.pdf>]. doi:10.1143/PTP.64.1103.
32. Glashow, S.L. The Future of Elementary Particle Physics. Quarks and Leptons; Lévy, M.; Basdevant, J.L.; Speiser, D.; Weyers, J.; Gastmans, R.; Jacob, M., Eds.; Springer US: Boston, MA, 1980; pp. 687–713.
33. Mohapatra, R.N.; Senjanović, G. Neutrino Mass and Spontaneous Parity Nonconservation. *Phys. Rev. Lett.* **1980**, *44*, 912–915. doi:10.1103/PhysRevLett.44.912.
34. Schechter, J.; Valle, J.W.F. Neutrino masses in  $SU(2) \otimes U(1)$  theories. *Phys. Rev. D* **1980**, *22*, 2227–2235. doi:10.1103/PhysRevD.22.2227.
35. Domin, P.; Kovalenko, S.; Faessler, A.; Šimkovic, F. Nuclear ( $\mu^- , e^+$ ) conversion mediated by Majorana neutrinos. *Phys. Rev. C* **2004**, *70*, 065501. doi:10.1103/PhysRevC.70.065501.
36. Atre, A.; Barger, V.; Han, T. Upper bounds on lepton-number violating processes. *Phys. Rev. D* **2005**, *71*, 113014. doi:10.1103/PhysRevD.71.113014.
37. Ejiri, H. Nuclear Matrix Elements for  $\beta$  and  $\beta\beta$  Decays and Quenching of the Weak Coupling  $g_A$  in QRPA. *Frontiers in Physics* **2019**, *7*, 30. doi:10.3389/fphy.2019.00030.

38. Vergados, J.D.; Ejiri, H.; Šimkovic, F. Theory of neutrinoless double-beta decay. *Reports on Progress in Physics* **2012**, *75*, 106301. doi:10.1088/0034-4885/75/10/106301.
39. Particle Data Group. Review of Particle Physics. *Progress of Theoretical and Experimental Physics* **2020**, 2020, [<https://academic.oup.com/ptep/article/2020/8/083C01/34673722/ptaa104.pdf>]. 083C01, doi:10.1093/ptep/ptaa104.
40. Abela, R.; Backenstoss, G.; Kowald, W.; Wüest, J.; Seiler, H.; Seiler, M.; Simons, L. New upper limit for  $\mu^- \rightarrow e^+$  conversion. *Physics Letters B* **1980**, *95*, 318–322. doi:https://doi.org/10.1016/0370-2693(80)90495-5.
41. Bertl, W.; Engfer, R.; Hermes, E.A.; Kurz, G.; Kozlowski, T.; Kuth, J.; Otter, G.; Rosenbaum, F.; Ryskulov, N.M.; van der Schaaf, A.; Wintz, P.; Zychor, I.; Collaboration, T.S.I. A search for  $\mu$ -e conversion in muonic gold. *The European Physical Journal C - Particles and Fields* **2006**, *47*, 337–346. doi:10.1140/epjc/s2006-02582-x.
42. Snover, K.A. Giant Resonances in Excited Nuclei. *Annual Review of Nuclear and Particle Science* **1986**, *36*, 545–603, [<https://doi.org/10.1146/annurev.ns.36.120186.002553>]. doi:10.1146/annurev.ns.36.120186.002553.
43. Kaulard, J.Q. Suche nach der Verbotenen Ladungsaustauschenden Mye-konversion  $\mu^- + Ti \rightarrow e^+ + Ca$  (Search for forbidden charge exchanging  $\mu e$  conversion  $\mu^- Ti \rightarrow e^+ Ca$ ). PhD thesis, RWTH Aachen university, 1997.
44. Dohmen, C.; Groth, K.D.; Heer, B.; Honecker, W.; Otter, G.; Steinrücken, B.; Wintz, P.; Djordjadze, V.; Hofmann, J.; Kozlowski, T.; Playfer, S.; Bertl, W.; Egger, J.; Herold, W.; Krause, B.; Walter, H.; Engfer, R.; Findeisen, C.; Grossmann-Handschin, M.; Hermes, E.; Muheim, F.; Niebuhr, C.; Pruys, H.; Ricken, L.; Vermeulen, D.; van der Schaaf, A. Test of lepton-flavour conservation in  $\mu \rightarrow e$  conversion on titanium. *Physics Letters B* **1993**, *317*, 631–636. doi:https://doi.org/10.1016/0370-2693(93)91383-X.
45. Ahmad, S.; Azuelos, G.; Blecher, M.; Bryman, D.A.; Burnham, R.A.; Clifford, E.T.H.; Depommier, P.; Dixit, M.S.; Gotow, K.; Hargrove, C.K.; Hasinoff, M.; Leitch, M.; Macdonald, J.A.; Mes, H.; Navon, I.; Numao, T.; Poutissou, J.M.; Poutissou, R.; Schlatter, P.; Spuller, J.; Summhammer, J. Search for muon-electron and muon-positron conversion. *Phys. Rev. D* **1988**, *38*, 2102–2120. doi:10.1103/PhysRevD.38.2102.
46. Badertscher, A.; et al.. New Upper Limits for Muon - Electron Conversion in Sulfur. *Lett. Nuovo Cim.* **1980**, *28*, 401–408. doi:10.1007/BF02776193.
47. Badertscher, A.; Borer, K.; Czapek, G.; Flückiger, A.; Hänni, H.; Hahn, B.; Hugentobler, E.; Kaspar, H.; Markees, A.; Moser, U.; Redwine, R.; Schacher, J.; Scheidiger, H.; Schlatter, P.; Viertel, G. Search for  $\mu^- \rightarrow e^+$  conversion on sulfur: A. Badertscher et. al., *Phys. Lett.* 79B (1978) 371. *Physics Letters B* **1979**, *80*, 434. doi:https://doi.org/10.1016/0370-2693(79)91214-0.
48. Badertscher, A.; Borer, K.; Czapek, G.; Flückiger, A.; Hänni, H.; Hahn, B.; Hugentobler, E.; Kaspar, H.; Markees, A.; Moser, U.; Redwine, R.; Schacher, J.; Scheidiger, H.; Schlatter, P.; Viertel, G. Search for  $\mu^- \rightarrow e^+$  conversion on sulfur. *Physics Letters B* **1978**, *79*, 371–375. doi:https://doi.org/10.1016/0370-2693(78)90385-4.
49. Bryman, D.A.; Blecher, M.; Gotow, K.; Powers, R.J. Search for the Reaction  $\mu^- + Cu \rightarrow e^+ + Co$ . *Phys. Rev. Lett.* **1972**, *28*, 1469–1471. doi:10.1103/PhysRevLett.28.1469.
50. Conforto, G.; Conversi, M.; Lella, L.d.; Penso, G.; Rubbia, C.; Toller, M. Search for Neutrinoless Coherent Nuclear Capture of  $\mu^-$  Mesons. *Il Nuovo Cimento* **1962**, *26*, 261–281. doi:https://doi.org/10.1007/BF02787041.
51. Abusalma, F.; et al.. Expression of Interest for Evolution of the Mu2e Experiment, 2018, [[arXiv:physics.ins-det/1802.02599](https://arxiv.org/abs/physics.ins-det/1802.02599)].
52. Bergbusch, P.C.; Armstrong, D.S.; Blecher, M.; Chen, C.Q.; Doyle, B.C.; Gorringer, T.P.; Gumplinger, P.; Hasinoff, M.D.; Jonkmans, G.; Macdonald, J.A.; Poutissou, J.M.; Poutissou, R.; Sigler, C.N.; Wright, D.H. Radiative muon capture on O, Al, Si, Ti, Zr, and Ag. *Phys. Rev. C* **1999**, *59*, 2853–2864. doi:10.1103/PhysRevC.59.2853.
53. Edmonds, A. Latest Updates from the AICap Experiment. 13th Conference on the Intersections of Particle and Nuclear Physics, 2018, [[arXiv:physics.ins-det/1809.10122](https://arxiv.org/abs/physics.ins-det/1809.10122)].
54. Yeo, B.; Kuno, Y.; Lee, M.; Zuber, K. Future experimental improvement for the search of lepton-number-violating processes in the  $e\mu$  sector. *Phys. Rev. D* **2017**, *96*, 075027. doi:10.1103/PhysRevD.96.075027.
55. Wong, T.S. Study of Negative Muon to Positron Conversion in the COMET Phase-I experiment. PhD thesis, Osaka university, 2020.
56. Kroll, N.M.; Wada, W. Internal Pair Production Associated with the Emission of High-Energy Gamma Rays. *Phys. Rev.* **1955**, *98*, 1355–1359. doi:10.1103/PhysRev.98.1355.
57. Joseph, D.W. Electron pair creation in  $\pi^+ p$  capture reactions from rest. *Il Nuovo Cimento* **1960**, *16*, 997–1013. doi:10.1007/BF02860383.
58. Plestid, R.; Hill, R.J. The high energy spectrum of internal positrons from radiative muon capture on nuclei, 2020, [[arXiv:hep-ph/2010.09509](https://arxiv.org/abs/2010.09509)].
59. Armstrong, D.S.; Serna-Angel, A.; Ahmad, S.; Azuelos, G.; Bertl, W.; Blecher, M.; Chen, C.Q.; Depommier, P.; von Egidy, T.; Gorringer, T.P.; Hasinoff, M.D.; Henderson, R.S.; Larabee, A.J.; Macdonald, J.A.; McDonald, S.C.; Poutissou, J.M.; Poutissou, R.; Robertson, B.C.; Sample, D.G.; Taylor, G.N.; Wright, D.H.; Zhang, N.S. Radiative muon capture on Al, Si, Ca, Mo, Sn, and Pb. *Phys. Rev. C* **1992**, *46*, 1094–1107. doi:10.1103/PhysRevC.46.1094.
60. Bergbusch, P.C. Radiative muon capture of oxygen, aluminum, silicon, titanium, zirconium, and silver. PhD thesis, University of British Columbia, 1995. doi:http://dx.doi.org/10.14288/1.0085124.



- 
61. Goringe, T.P.; Armstrong, D.S.; Chen, C.Q.; Christy, E.; Doyle, B.C.; Gumplinger, P.; Fearing, H.W.; Hasinoff, M.D.; Kovash, M.A.; Wright, D.H. Isotope dependence of radiative muon capture on the  $^{58,60,62}\text{Ni}$  isotopes. *Phys. Rev. C* **1998**, *58*, 1767–1776. doi:10.1103/PhysRevC.58.1767.
  62. Christillin, P.; Rosa-Clot, M.; Servadio, S. Radiative muon capture in medium-heavy nuclei. *Nuclear Physics A* **1980**, *345*, 331–366. doi:https://doi.org/10.1016/0375-9474(80)90344-9.
  63. Fearing, H.W.; Walker, G.E. Radiative muon capture in a relativistic mean field theory: Fermi gas model. *Phys. Rev. C* **1989**, *39*, 2349–2355. doi:10.1103/PhysRevC.39.2349.
  64. Fearing, H.W.; Welsh, M.S. Radiative muon capture in medium heavy nuclei in a relativistic mean field theory model. *Phys. Rev. C* **1992**, *46*, 2077–2089. doi:10.1103/PhysRevC.46.2077.
  65. Kitano, R.; Koike, M.; Okada, Y. Detailed calculation of lepton flavor violating muon-electron conversion rate for various nuclei. *Phys. Rev. D* **2002**, *66*, 096002. doi:10.1103/PhysRevD.66.096002.
  66. Cirigliano, V.; Kitano, R.; Okada, Y.; Tuzon, P. Model discriminating power of  $\mu \rightarrow e$  conversion in nuclei. *Phys. Rev. D* **2009**, *80*, 013002. doi:10.1103/PhysRevD.80.013002.
  67. Mohr, P.J.; Newell, D.B.; Taylor, B.N. CODATA recommended values of the fundamental physical constants: 2014. *Rev. Mod. Phys.* **2016**, *88*, 035009. doi:10.1103/RevModPhys.88.035009.
  68. Czarnecki, A.; Garcia i Tormo, X.; Marciano, W.J. Muon decay in orbit: Spectrum of high-energy electrons. *Phys. Rev. D* **2011**, *84*, 013006. doi:10.1103/PhysRevD.84.013006.
  69. Wang, M.; Audi, G.; Kondev, F.G.; Huang, W.; Naimi, S.; Xu, X. The AME2016 atomic mass evaluation (II). Tables, graphs and references. *Chinese Physics C* **2017**, *41*, 030003. doi:10.1088/1674-1137/41/3/030003.
  70. Suzuki, T.; Measday, D.F.; Roalsvig, J.P. Total nuclear capture rates for negative muons. *Phys. Rev. C* **1987**, *35*, 2212–2224. doi:10.1103/PhysRevC.35.2212.